Microprobe U-Th-Pb_T Dating of Monazite: Top-Down, Bottom-Up or *au Rebours*?

Gavril Săbău and Elena Negulescu, *Members, GSTF*

***Abstract* — Extensive statistical characterization of individual analyses, supported by chemical data, represents a highly effective alternative in microprobe chemical dating of monazite, preventing possibly arbitrary *a priori* grouping of analyses. Age values and associated errors obtained for each analysis by error propagation through an explicit approximation of the age equation allow accurate subsequent statistical processing in order to identify consistent and meaningful populations. A procedure that involves seeking out of coherent clusters in complex age spectra, assessment of the overall probability distribution function, its deconvolution, and chemical correlations opportunely complements the high spatial resolution of the microprobe analyses, potentially highlighting the timing, context and duration of intricate events and processes in the thermotectonic evolution of igneous and metamorphic rocks.**

***Index Terms* — Geochronology, Monazite, Microprobe analyses, Age spectra processing, Deconvolution**

I. Introduction

MONAZITE chemical U-Th-Pb_T geochronology has recorded a continuous development over the past two decades, followed by a considerable boom in the last few years. Its main strong points are related to a truly *in situ* and non-destructive character and a high spatial resolution, which ideally translate in a temporal resolution enabling determination not only of age, but also of duration of metamorphic and magmatic events, provided a sufficient precision and accuracy of the measurements are ensured.

The main drawbacks of the method originate in using a chemical method as a proxy for isotopic dating, and in applying an analytical technique originally designed for major elements for measuring trace element concentrations. Using concentrations of radioactive elements and their decay products for age calculations is based on the assumption that the isotopic system contained negligible (or predictable) quantities of daughter elements (Pb in this case) at the time of monazite crystallization, and that the isotopic equilibrium persisted undisturbed during the subsequent evolution of the host rock. On the other hand, low concentrations of the measured elements directly reflect in poor analytical statistics and consequently low precision and accuracy under normal working conditions.

Since monazite was confirmed to contain negligible common lead both by attempting to calculate initial lead from isochrons on coeval populations [1], [2] and by direct analyses [3], increasing efforts to enhance the quality of microprobe analyses appeared justified and contributed to a continuous improvement of the method. Several aspects pertaining to the quality of the microprobe analyses were carefully addressed, starting from sample contamination [4], matrix effects [5], resolving peak overlaps and establishing background levels [6], all influencing the precision of the measurements, as well as careful selection of measured peaks, instrumental conditions ensuring high count rates, and suitable standards, all with direct effect on the accuracy. On the other hand, detailed studies of the mechanisms by which monazite age resetting occurs provided a better understanding of within-grain age distributions, as well as additional support to the key assumptions underlying monazite microprobe chemical dating, namely negligible primary lead and isotopic equilibrium during post-crystallization evolution [7]. Another important progress is the availability of reliable and well characterized age and compositional standards, such as the Moacir monazite [8].

Despite important progress achieved in handling the accuracy and precision issues of the U-Th-Pb microprobe analyses, the U-Th-Pb_T monazite dating method still lacks well-established and widely-employed analytical approaches and data processing schemes, similar to those adopted for isotopic dating methods, and enabling rigorous comparison among data originating from different laboratories [9]. The weak points saliently emerging from the relevant literature appear to be a few missing links on the way from microprobe analyses to geologically relevant age populations, resulting from rigorous statistical processing and characterization. Error handling and propagation assessment from chemical analyses to age data is inherently deficient if age values are obtained, as in most instances, by iterative solving of an implicit age equation (*e. g.* [10]). On the other hand, there is still a poor definition of objective criteria for recognition and separation of relevant populations within the analytical sets in order to perform a well-aimed statistical analysis of the results.

Using a terminology borrowed from the field of software

Manuscript received February 28, 2013. This work was supported by the Romanian Executive Unit for Financing Higher Education, Research, Development and Innovation (UEFISCDI) under Grant PN-II-ID-PCE-2011-3-0030.

G. S. is project manager with the Geological Institute of Romania, 1 Caransebeş St., RO-012271 Bucharest 32, Romania (phone: +40-21-3060451; fax: +40-21-3181326; e-mail: g_sabau@ yahoo.co.uk).

E. N. is senior researcher with the Geological Institute of Romania (e-mail: elinegu@yahoo.com).

DOI: 10.5176/2335-6774_1.1.3

development, two different approaches in handling U-Th-Pb_T analyses for chronological purposes have been distinguished [9]: the "top-down" analysis, involving large groups of analyses from which individual populations and pertaining data are extracted by means of statistics, and the "bottom-up" strategy, starting from individual compositional domains, and combining the results in order to characterize the history of the whole analyzed sample. The latter approach treats spot analyses rather like cycles of an individual measurement than separate age data [9]; instead an age datum is referring to a whole domain found to be chemically homogeneous by elemental mapping of the monazite grains from the sample. In fact, both such defined approaches have in common the fact that individual analyses are not processed separately, being rather incorporated in populations for which the separation criteria might be arbitrary, the difference between the two approaches becoming rather fuzzy. In our opinion, a truly "bottom-up" approach has to consider individual analyses, in order to fully take advantage of the very high spatial resolution of the method and to translate it as much as possible in terms of temporal resolution. Individual age data should be combined into age domains, and the results extended over samples, rock types and formations.

II. From Spot Analyses to Age Data

A. Current Approaches

A more useful and realistic classification of the monazite chemical geochronological approaches would be the way in which data are obtained and statistically handled, namely if the age measurements are assessed individually and subsequently grouped, or are a priori grouped in populations which are then statistically evaluated. Isochron methods inherently require predefined populations, while the "bottom-up" [9] approach uses by-choice grouping according to chemistry and zonality of the investigated grains. Statistic evaluation of the individual analyses relies on the probability distribution function, while the isochron methods perform a statistical evaluation of the isochrons themselves.

Critical aspects common to both approaches are the error propagation from chemical data to age data, and the appropriate grouping of individual spot analyses into domains or coherent populations in order to extract geologically relevant information. These issues are handled differently by each of the approaches applied in chemical monazite chronology.

The CHIME [11] method groups a number of analyses and derives a pseudo-isochron in the PbO *vs*. ThO_2* (or UO_2*) space. This operation assumes the coeval character of the individual analyses, which may hold true in case of inspired or iterative selection of point data. Two shortcomings affect the method, namely the use of an estimated value for A_{Pb} to iteratively calculate the value of ThO_2* when refining the pseudo-isochron, and the implicit assumption of a unique quantity of common lead in all point data, corresponding to the intersection of the pseudo-isochron with the Pb ordinate, which is by no means realistic (see also [10]), unless this quantity equals zero. As the intercept of the pseudo-isochron is located in the point of origin in the overwhelming majority of case studies [2], the method shows on one hand that differing compositions are often perfectly coeval, and on the other hand provides evidence that common lead in monazite is usually negligible as compared to radiogenic lead.

The isochron method using the Th/Pb = f(U/Pb) diagram [12] provides certain advantages both in error handling because only the elemental errors and their ratios are propagated through the formalism, and in selection of samples because grouping is highly facilitated, besides statistical assessment, also by visual inspection of the diagram. The precision of the method is highly dependent on the scatter in U/Th among spot data. For this reason, different strategies are proposed [13] according to the U-Th systematics: the Th/Pb = f(U/Pb) isochron for significant variations in the Th/U ratio, the Pb = f(Th*) pseudo-isochron for a fairly constant Th/U ratio, but significant U+Th heterogeneity, and a simple weighted average for a population displaying constant U and Th concentrations.

Irrespective of the U-Th systematics, a coherent strategy based on statistical processing of individual spot data is proposed by [10]: age error estimation by propagation of the elemental errors through the age equation (which is basically a Pb balance equation, not influenced by the actual atomic mas of lead, and relates element concentration to age values through an implicit expression), calculation of a weighted age histogram by summation of the individually calculated probability distributions, selection of data by a trial and error least squares modelling, and pooling the selected analyses in narrower age domains for which averages and standard deviations can be calculated. The shortcomings of the workflow as exposed in [10] are: possibly inaccurate error propagation assessment through an implicit expression, a somewhat obscure procedure of pooling point data, and inconsistent scaling of the probability plots.

In the procedure defined as "bottom-up" [9] average element contents are obtained from multiple analyses and for each element a mean and the standard deviation of the mean are calculated and then propagated through the age equation of [10], considering the combination of several spot analyses as a single datum. This implies that chemically homogeneous domains are also coeval, which is indeed the most probable case. However, compositional domains are not always equivalent to individual age domains, because the composition of individual grains or zones may not be the result of bulk equilibration in the rock; instead they may form during local or mosaic equilibration, depending on the precursor phases and accompanying minerals which partition cations with monazite, either major phases containing them in trace amounts, or accessory phases containing them as main components (see also [14]). It is highly probable for coeval monazite domains to display contrasting compositions, and it is possible to record similar compositions in grains formed at

different times in the history of the rock. Therefore analyses grouping that relies on element distribution maps alone may obscure features otherwise apparent only due to the high resolution of the microprobe point analysis. As regards the precision, despite the fact that the standard error of the mean assumes lower values than the standard deviation of a population, these parameters are not equivalent, thereby the higher precision obtained being only apparent. The procedure also does not improve the approximation of the age error, since it is estimated by mere propagation through an implicit equation.

An extension of the "bottom-up" approach over complex age spectra is given by [15], as also an upgrade on the bottom-up vs. top-down terminology. Accordingly, a bottom-up approach consists in pooling analyses, as opposed to separating age populations from all analyses. Pooled analyses are processed as mentioned above, and the overall age spectrum is represented in a diagram called "relative probability plot", which is calculated in a similar way to a probability density plot, except that once again the standard deviation of the pooled means are substituted for the standard deviation of each population. The sharp maxima of the plot are invoked in support of a much better precision than in case of statistically processing individual spot analyses. In fact, the results appear to be strongly biased by the number of spot analyses in each pooled age cluster, in a way related rather to the questionable calculation of the confidence level than to the moment when analyses are pooled, *a priori* or *ad posteriori*.

From the overview of the currently applied monazite chemical dating techniques, the method outlined in [10] distinguishes itself by its applicability regardless of the U/Th ratio or zonality of the monazite grains, being also unbiased by inhomogeneous weighting of spot analyses according to the number of pooled analyses. The applicability and reliability of the method can significantly expand, given a few improvements concerning error propagation assessments from analytical uncertainties to age confidence levels, an accurate representation of the probability distribution inside a population, criteria for separating coherent populations from mixed data, and independent supporting evidence.

B. Problems and proposed solutions in data processing

For optimal statistical handling of data, it is highly desirable to define individual analyses as clearly as possible in terms of values and errors. Comparison of individual values with results of other laboratories and/or data derived by other methods can only occur after compensation of systematic errors and evaluation of random errors, by presenting the age data as values and associated standard deviations. This requirement cannot be fulfilled if ages are calculated using an implicit formula which prevents rigorous error propagation assessment from concentration data to age values. The solution is given by precise explicit approximations of the age equation, enabling also the estimation of the associated age errors [16] and making possible a sound further statistical evaluation.

In full agreement with [10], the most adequate way of evaluating populations composed of several spot analyses is the calculation of the probability density function, which, however, is not a histogram and is, or should be, rather normalized than weighted. Unfortunately, the way in which this procedure is illustrated in the mentioned paper does not match the specifications given in text. As an example, the diagram in Fig.1 was plotted according to the method indicated by the authors, using the data given for the Velay granite, while the inset on the left reproduces Fig. 1 (a) in the cited paper.

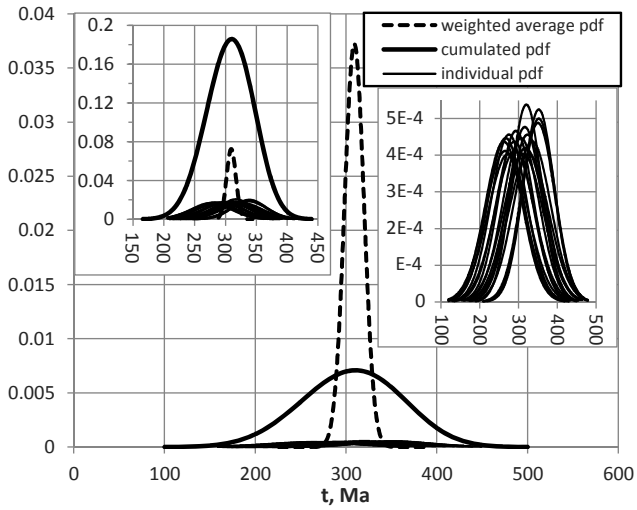

Fig. 1. Probability distribution function (pdf) representations of the example given in [10], fig. 1(a) and corresponding data. Inset on the right is a detail scaled to view the individual probability plots. Inset on the left is an attempt to match the source illustration for comparison. Note inconsistent both abscissa and ordinate scales.

The graph presented therein can be reproduced only by multiplying the plots by arbitrary coefficients (in this case by 2 for the unnormalized individual plots, their summation by an additional factor of 0.69, and again by 2 for the weighted average probability plot), and additionally contracting the whole graph as compared to the abscissa scale by a factor of about 0.66 both sides away from the mean value. The integral of each plot in [10], Fig. 1 (a) yields 2, except for the "weighted histogram", which integrates up to some quantity exceeding 26. Instead, in order to maintain consistency among the different graphs, one has to normalize each individual probability plot by dividing its value by the number of samples, which leads to an integral of the overall probability distribution function (= their sum) equalling 1. By extension, in case of pooling spot data in several clusters, each characterized by an average and standard deviation, the probability function has to be normalized by a factor equalling the fraction that cluster represents from all data. Then the integral of the summed probability functions of all cluster averages would equal 1. The relative low relevance of distinguishing the point data probability distribution functions as well as the low values assumed by them on probability distribution graphs (Fig. 1) makes preferable to skip calculating these functions, calculating instead directly the

overall probability function. Given the ages and standard errors of the spot data $t_1 \ldots t_n$ and $\sigma_1 \ldots \sigma_n$ respectively, an interval (t_l, t_h) in which the probability distribution function assumes significant values, and the argument $t \in (t_l, t_h)$, the value of the normalized overall probability function at age t is:

$$\Phi(t) = \sum_{i=1}^{n} \frac{1}{n\sigma_i \sqrt{2\pi}} e^{-\frac{(t-t_i)^2}{2\sigma_i^2}}, \text{ and } \int_{t_l}^{t_h} \Phi(t)dt = 1.$$

In an Excel table the expression is written as an array function, "{=SUM(EXP(-((t-t_1$:$t$_n$)^2/2/$σ$_1$:$σ$_n$^2))/$σ$_1$:$σ$_n /SQRT(2*PI()))/COUNT($t$_1$:t_n$)}" where t_1:t_n and $σ_1$:$σ_n$ stand for the cell arrays in which spot ages and associated standard errors are stored.

Pooling analyses in consistent groups is a key challenge of data synthesis. Two procedures of are usually employed, separating analyses on a purely statistical basis [10], or *a priori* selection of the population based on chemical criteria [9]. Instead of iteratively testing statistical parameters in random groups, judicious pooling of analyses may benefit from a rather simple graphical treatment. A population coherently grouping around a significant age value is expected to follow the normal distribution law around the most probable value. The plot in Fig. 2 represents a simulated set of ages displaying normal (Gaussian) distribution with number of samples n = 51, mean (μ) of 300 Ma and standard deviation of the population σ = 1, sorted in increasing age order. Remarkable is the sigmoidal shape, reflected also in the variation of the age gradient between individual values (inset C in Figure 2), which assumes a concave-upwards pattern.

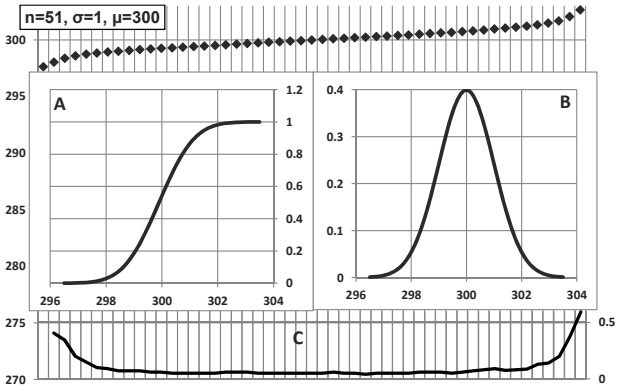

Fig. 2. Gaussian distribution of generated age values; statistical parameters (see also text) described in label upper left. Insets represent the cumulative curve (A), the probability distribution function plot (B - relative abundances on the ordinate) and the gradient of the age values, expressed simply by the difference between two consecutive ages (C).

This variation is in many instances easily recognized in sorted age patterns, allowing separation of coherent age groups which may have geological relevance from an otherwise complex age spectrum. The age-sorted plot of the individual point data, together with the standard deviations of the measurements and the age gradient, expressed this time as a normalized value (the difference between two consecutive ages divided by the averaged standard errors) represents a simple but valuable tool in selecting possibly single-age domains, as it also gives an often surprisingly clear image of the age distributions in a dataset. The separation of the domains can be facilitated by setting a corresponding threshold value for the maxima in the age gradient, in most often cases in the range of 0.5-0.75. The point data in the resulting domains are pooled resulting in refined age values. Depending on the density and relative overlaps of the probability curves associated to the pooled averages, they may mark separate events or stages in a protracted episode of monazite formation. The pooled maxima also allow a full deconvolution of the probability distribution graph by a mere iterative increasing adjustment of the standard error of each pooled cluster. This operation can be achieved graphically by programming the residuals, as will be illustrated in the worked examples given later on. It is to note that the weighted averages of the pooled age domains, in order to deliver meaningful results and allow a precise deconvolution, have to assume very low MSWD values and very high probabilities of fit.

C. Age domains and compositional domains

The characteristic feature of chemical dating of monazite is represented by using the concentrations of elements belonging decay series as a proxy for isotopic ratios. On the other hand, chemical data obtained during microprobe analyses offer a by far wider potential than the possibility of statistically processing calculated ages. The recognition and definition of coherent compositional domains and their relationship to age domains is essential for correctly grouping the data and obtaining geologically relevant age values. In this respect, the importance of element distribution maps is clearly pointed out [9]. Yet, by using distribution maps alone, much of the information gathered during microprobe analyses dissipates in the background; therefore a better approach is to consider also chemical data obtained during the analytical process [7]. Though some authors recommend separate microprobe sessions for major elements and trace elements [9], it is perfectly feasible, using adequate instrumental configuration, to measure all elements, with the advantage that one doesn't need to use results of a separate session in order to approximate the matrix effects, and by doing so direct criteria are provided to estimate the quality of the analyses, such as the recalculated totals or stoichiometry. Chemical characterization of monazite populations is an essential step towards turning the chemical monazite geochronology into a multi-proxy approach, in which statistical, chemical, zonality and textural analysis support each other and provide a solid substantiation to geological reasoning. Qualitative determination, from mineral assemblages and textural setting, of the nature and relative timing of the monazite forming events, combined with understanding the way monazite compositions change in response to element partitioning and fractionation during processes such as mineral reactions [17], [14], melting [18], [19], growth and resorption [20] may provide valuable criteria in evaluating monazite compositional

features and their evolution in time.

Compositional features and trends of monazites can be conveniently characterized on normalized chemical plots, using as a normalizing factor either widely-employed standards as element abundances in chondrites [21], [22], or a standard composition included in the population itself [23]. Very useful are also ternary plots reflecting the relative abundances in LREE, Y, M+HREE and U+Th+Ca in order to highlight the substitutions occurring in monazite and their variation trends. Normalized lanthanide concentrations are also effective in deriving more quantitative data, such as element ratios pertaining to the fractionation of elements in monazite or partition with their geochemical environment, such as Ce/Nd, Nd/Gd, Gd/Y, besides the U/Th ratio, as well as enrichment-depletion markers such as $Eu^{*2} = Sm \times Gd$, $Y^* = Dy^2/Gd$. Processing of chemical data may in favourable cases result in differentiating distinct populations, which can be examined in correlation with the corresponding age variations.

III. Worked Examples

The procedure of separating discrete populations from the distribution of the age data will be exemplified in comparison with previously published data using a similar approach, and by processing original data in connection with the chemical features of the analyzed grains.

Reference [24] applies microprobe monazite dating following the data processing procedure outlined in [10], on several rock types from the Kerala Khondalite Belt of southern India, among which a khondalite sample displaying a complex age spectrum (sample K35).

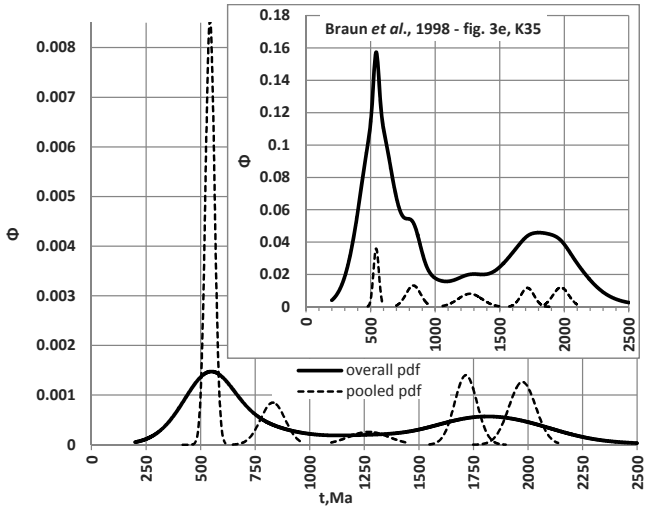

Fig. 3. Calculation of the probability density functions (pdf - Φ) for the U-Th-Pb data reported in [24], using the same data pooling. Inset represents an attempt to reproduce the same plots as represented in the original paper. Probability expressed in dimensionless units.

The probability density functions for the entire dataset and the groups pooled by the authors are plotted in Fig. 3. For comparison we present an attempt to duplicate the original figure, displaying notable inconsistencies in scaling among the different curves, none of which integrating to a probability of 1. Values and graph patterns closer approximating the mentioned illustration could be obtained only by using unnormalized probability plots for the pooled selections, multiplied arbitrarily, as well as an arbitrary linear combination among these and the individual data, though the "weighted histogram" is not supposed to include pooled data.

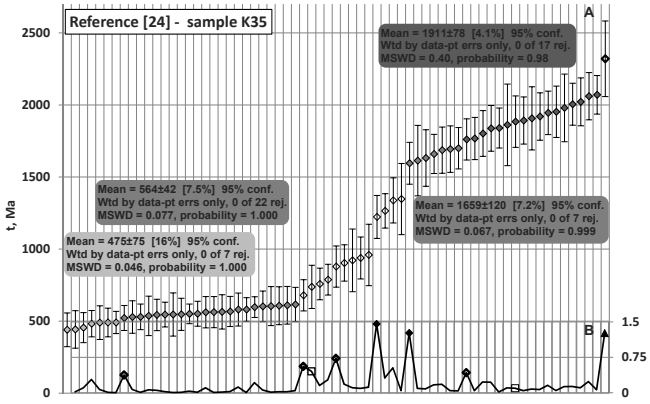

Fig. 4. Age distribution plot (A) and normalized age gradient (B) for sample K35, used to separate age groups for pooling. The boundaries of the age groups are represented in (B), using filled diamonds for group boundaries maintained from [24] and empty diamonds for newly selected boundaries. Age group boundaries discarded are marked with empty squares; analysis marked with filled triangle was not included in the evaluation. Selected age domains are distinguished by signature and labelled indicating statistical parameters of the weighted averages calculated with the Isoplot 4.15 Excel add-in [25].

A somewhat different data pooling was conducted using the age-sorted graph and the normalized gradients (Fig. 4), plotted after recalculation of the ages and errors according to [16]. The values thus obtained do not differ significantly as compared with values given in [24].

The normalized gradients in the age-sorted plot allow a finer grouping of the age data than more or less "blind" statistical testing; as a result the composite structure of the cluster in the 600-1000 Ma interval and an additional cluster at ages younger that 500 Ma become visible. The former age range displays a marked scattering with a tendency to better grouping at higher age values, while the latter contain mainly rim compositions clearly departing from the quasi-plateau slightly above 500 Ma. One analysis was excluded from grouping, as it clearly represents a high-error outlier at the older end of the age pattern. The calculated statistical parameters of the weighted averages of each cluster display very low MSWD values; a more permissive grouping would result in overlaps of the pooled probability function plots, as well as high residuals of the age spectrum deconvolution. Empirically, MSWD values about 0.5 correspond to the lowest admissible precision limit.

Plotting the probability distribution function of the entire population besides the same function for each pooled cluster for which the weighted average and associated error were calculated separately and normalized in order to obtain a summed probability of 1 for the entire population, a pattern

displaying many similarities, but also some differences when compared to Fig. 3.

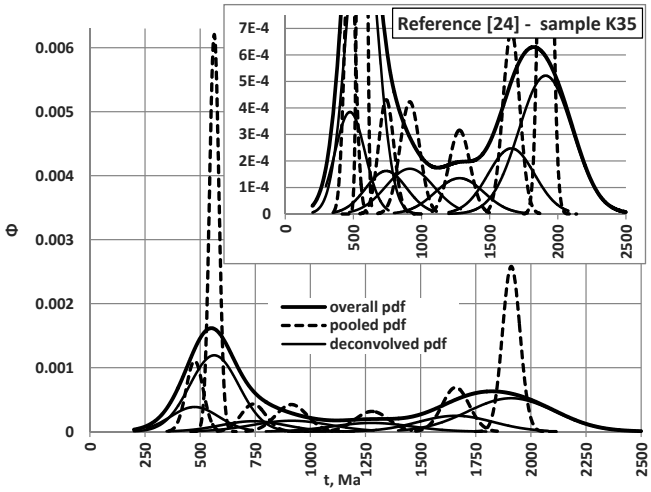

Fig. 5. Probability distribution plots for the entire dataset, pooled clusters and deconvolved components of the summed probability function, centered on the averages of the pooled clusters. Inset represents an enlargement of the lower part of the graph.

Both the absolute and relative amplitude of the individual probability plots of the pooled age domains is modified, outlining two important maxima, around 1900 and 560 Ma, which dominate the age spectrum. (Fig. 5).

The full deconvolution of the probability distribution plot starting from the domain averages of the pooled values by iteratively adjusting the standard error of each domain results in the graph in Fig. 5. The deconvolution is achieved by mathematical programing of the residuals as a function of individual standard errors. For the sample analyzed, the distribution of the residuals after optimization is plotted in Fig. 6.

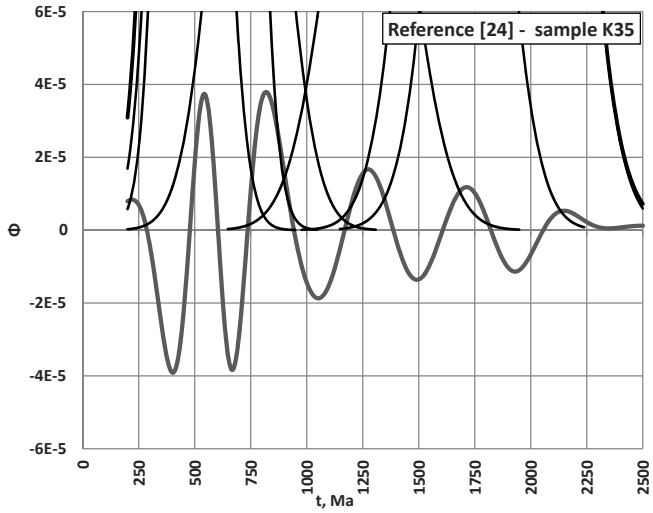

Fig. 6. The deconvolution residuals of the probability distribution plot for the analyzed sample. The overall probability distribution and its deconvolved components appear truncated in the upper part of the graph.

The optimization was accomplished by obtaining a symmetrically oscillating pattern of decreasing amplitude, which corresponds to a minimum area of the residuals, equalling 0.027 (probability units). The parameters resulting from the refinement are tabulated in Table 1. The age clusters

TABLE I
AGE DATA REFINEMENTS FOR SAMPLE K35

t, Ma	Pooled clusters					Deconvolved ages		
	σ	n	Δ	σ_Δ	SDμ	σ	σ_Δ	SDμ
475	38.27	7			14.46	110		42
564	21.43	22	89	43.86	4.57	111.5	156.63	24
741	56.12	4	177	60.07	28.06	149	186.1	75
914	71.43	5	173	90.84	31.94	177	231.37	79
1279	76.53	4	365	104.69	38.27	179	251.73	90
1659	61.22	7	380	98.01	23.14	171	247.55	65
1911	38.8	17	252	73.02	9.65	197	260.86	48

n - number of analyses, Δ - interval between two consecutive age values and its standard error σ_Δ, SDμ - standard deviation of the mean

are perfectly resolved at a confidence level of 95% using the pooled averages, with the exception of the clusters at 714 and 914 Ma, which however are resolved at 1σ level ($\Delta > \sigma_\Delta$). Using the deconvolved clusters, only the maxima at 1279 and 1659 Ma are resolvable.

In Table I the standard errors of the mean values have been calculated in order to allow a comparison with the approach presented in [9], especially the high precision claimed by using the standard deviation of the mean as a measure for age determination errors. In this way not only the precision of individual data is obnubilated, but also the statistical spread of the data gets confused with the precision of the mean. Estimating the standard error of the mean is rather a measure of the accuracy than of precision, and a sizeable part of this accuracy is represented by the "accuracy" of data selection. From the data in Table I, according to the deconvolved probability plot, which represents a rather robust statistical assessment, not only a group of data spread around a mean value of 1279 Ma with a standard deviation of 179 Ma, but also the position of the mean is calculated with an expected 1σ error of 90 Ma. By considering the pooled values and the standard error of the mean, one could engender the false impression that for the same data a precision of 38.3 Ma can be derived from 4 spot analyses with individual standard errors averaging 160 Ma, spread over an interval of 114 Ma.

The results support and supplement the conclusions already presented in [24]: the main thermotectonic events recorded correspond to an Early Proterozoic stage around 2 Ga and a dominant Late Proterozoic overprint around 564 Ma, while the data for the interval in-between remain poorly-constrained and not supported by alternative evidence, as also whether the intermediate ages obtained reflect protracted cooling or, alternatively, discrete events. Yet, a good clustering is apparent for the data around 914 Ma, suggesting at least one separable event. On the other hand, the data also support an Ordovician stage, identified with certainty in other rock types, but not recognized by [24] in khondalites.

A second example refers to a rock from the Leaota Massif, Romania, for which petrologic and structural evidence supports a polystage metamorphic history [26]. The investigated rock appears in the footwall and enclaves of the Albești metagranite, for which [27] report an U-Pb protolith

age of 472.7±7.3 Ma. The rock consists of a fine-grained groundmass containing idiomorphic porphyroblasts, reacted to kyanite paramorphs after andalusite and garnet-phengite fine-grained intergrowths, subsequently partly deformed and retrogressed. The qualitative metamorphic history indicated is contact metamorphism followed by low differential strain tectonical thickening, then by cooling and decompression under a high-strain regime.

Monazite is relatively abundant in the groundmass, displaying a complex and variable zonality with concentric, irregular, embayed and truncated aspects. No significant inclusion and textural relationships could be recorded in order to directly relate monazite growth stages to surrounding metamorphic assemblages. We analyzed chemical compositions in a sample (LTg2) using the five-detector Cameca SX100 microprobe of the Institute of Mineralogy and Crystal Chemistry in Stuttgart. Major and minor elements

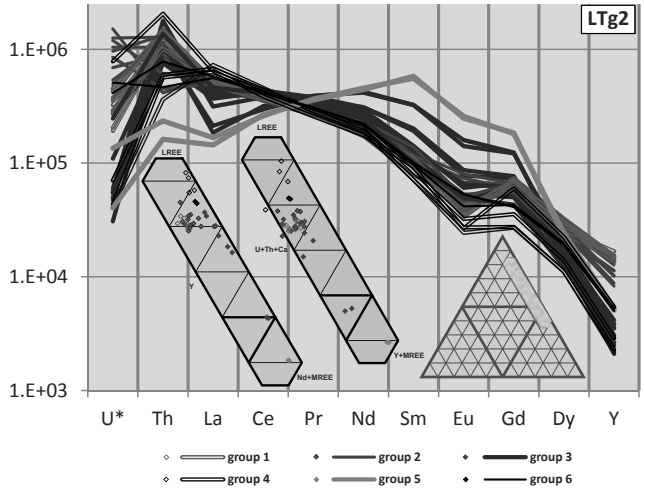

Fig. 7. Chondrite-normalized [21] (CN) and ternary cationic plots (atoms p.f.u.) of monazite from sample LTg2. U* represent U Mβ concentrations corrected for Th interference. Position of ternary fields represented in the insets on the lower part of the figure marked on the ternary template inset lower right.

were recorded simultaneously using an accelerating potential of 20 kV, a beam current of 200 nA, and different peak and background counting times according to the abundance of the analyzed elements, for both chemical assessment and geochronological purposes. The results are summarized in Fig. 7 and following.

From the chemical plots in Fig. 7 six different compositional groups may be distinguished. Group 1 displays the best compositional clustering, most uniform lanthanide pattern and highest Y content; group 2 of somewhat similar composition has lower Y, higher and variable $(U/Th)_{CN}$ ratio, and a variable and lesser negative Eu anomaly. The other 3 groups are depleted in Y and range between Ce+La+Pr – rich composition (group 4) and marked Nd+Sm enrichment (Nd>Ce>Sm>La in absolute concentration - group 5). Group 3 and 4 display the highest relative Y depletion, group 3 also having a higher brabantite substitution and a negative La anomaly. Subordinate group 6 has higher Y than groups 3 and 4, $(U/Th)_{CN} \approx 1$ and the slightest Eu anomaly. In the ternary plots in Fig. 7 Nd was included lumped together with the MREE group because of its behaviour. The correlation reversal in the lanthanide contents with increasing atomic number tends to be variable in different monazite population, occurring somewhere between Pr and Sm, but more often Nd positively correlates with heavier lanthanoids rather than with Ce. Variable correlations among lanthanoids appear to be frequent in metamorphic monazites, most probably being related to complex and insufficiently elucidated partition mechanisms with coexisting mineral phases (major and accessory phases alike), but also being potentially influenced by the relative mobility of the cations and the kinetics of the mineral reactions involving monazite.

It is apparent (Fig. 8) that the different chemical groups correlate well with the position of the corresponding spot data in the age-sorted plot. Compositional changes generally correspond to high-gradient points and represent suitable and

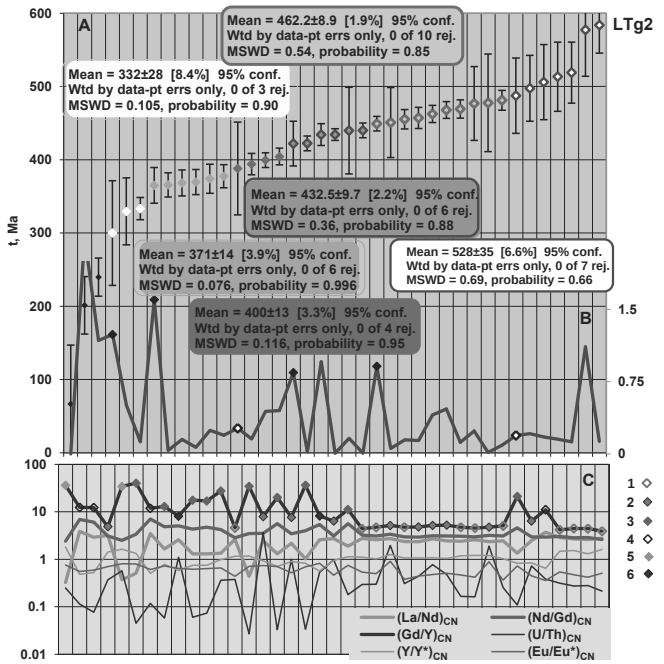

Fig. 8. Age distribution plot (A), normalized age gradients (B) and chemical indices (C) of the spot data. Selected age domains in A distinguished by signature and labelled to indicate statistical parameters. Markers in B correspond to domain boundaries, represented differently in case of high- and low-gradient boundaries. Signatures in C correspond to chemical groups distinguished in Fig. 7.

potentially significant boundaries for data pooling. In the two cases in which the change in the compositional features is not accompanied by significant gradient variations, the adjacent spot data have high errors, and were nevertheless selected as domain boundaries. One high-gradient value was not selected as domain boundary because it does not correspond to a compositional variation, occurring also between two low-error spot data.

The data plotted in Fig. 8 allow the distinction of 6 age domains, supported also by the chemical features. The oldest age domain is remarkably homogeneous, being represented by group 1 compositions with constant element ratios, marked Eu negative anomaly, high and constant Y contents, with Y/Y*

marking Y enrichment with respect to medium and heavy lanthanoids, gradually increasing $(U/Th)_{CN}$, which all suggest bulk-rock equilibration with a Ca-bearing phase, partition with an additional LREE-bearing phase, continuous breakdown of an accompanying U-bearing phase and lack of significant garnet growth. The age domain ends with a chemically variable set represented by 3 data point showing relative Y depletion, which can be interpreted as growth under bulk-rock disequilibrium, coevally with episodic garnet growth. The largest- represented age domain (2) consists of compositions belonging to groups 1 and 2 (low-Eu compositions), displaying also a marked compositional homogeneity except for fluctuating U/Th ratios; the Eu negative anomaly is well defined and constant, while relatively high Y does not differ in behaviour with respect to medium and heavy lanthanoids. These features are consistent with bulk-rock equilibration, Eu fractionation and no notable garnet growth. Age domains 3 and 4 contain spot analyses belonging to groups 2 (high-Eu compositions) and 3, displaying heterogeneous compositions with insignificant Eu anomaly and Nd-enriched with respect to La and Gd in comparison to age domain 2. Both Gd and Nd increase with respect to La. Age domain 4 appears relatively Y depleted, possibly indicating the onset of a new garnet growth episode. Age domain 5 appears chemically homogeneous and contains analyses from chemical group 3 moderate Eu anomaly, Y-depleted and recording a slight but constant increase in lighter lanthanoids. The chemical variation in age domain 5 are consistent with the main garnet-forming episode. Age domain 6 encompasses the MREE-richest compositions (including Nd and Sm) of groups 3 and 5, with low Y, but a relative Y enrichment relative to MREE. A similar unusual Nd and Sm enrichment was described by [20], related to detrital monazite resorption, along with minor

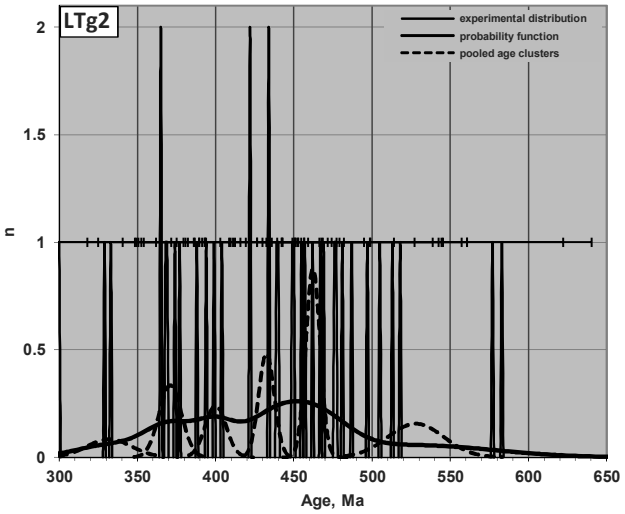

Fig. 9. Plot of the age data pertaining to the analyzed sample, displaying individual spot data, associated errors, the overall probability distribution plot and the probability distribution functions of the pooled domains

neoformation of high-LREE monazite, interpretation which can be extended, despite differences in context, to the analyzed sample, considering also the coeval high-LREE chemical group 4. Scattered low-precision analyses at the lower age extremity of the age pattern were not considered for age domain grouping.

Considering the age domains defined as above, we conducted a statistical assessment (Fig. 9-10). Fig. 9 displays

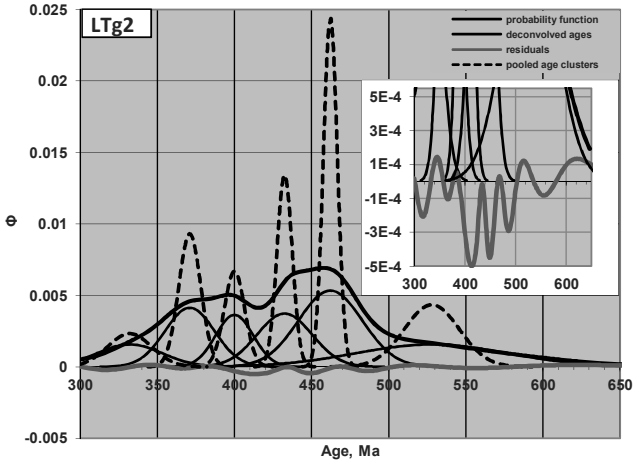

Fig. 10. Full deconvolution of the probability distribution plot starting from the probability distribution in the selected age clusters. Inset displays a vertically-enlarged view showing the residuals of the fit.

the location and frequency of individual spot data along with the probability distribution function derived for the overall population and the age domains separated using the age gradients and chemical features of the spot analyses.

The deconvolution of the overall probability distribution plot in Fig. 10 was obtained from the position of pooled

TABLE II
AGE DATA REFINEMENTS FOR SAMPLE LTG2

t, Ma	Pooled clusters					Deconvolved ages		
	σ	n	Δ	σ_Δ	SDμ	σ	σ_Δ	SDμ
332	14.29	3			8.25	21.2		12.24
371	7.14	6	39	15.97	2.92	16.077	26.61	6.56
400	6.63	4	29	9.75	3.32	12.195	20.18	6.1
432.5	4.95	6	32.5	8.28	2.02	17.85	21.62	7.29
462.2	4.54	7	29.7	6.72	1.44	20.77	27.39	6.57
528	17.86	10	65.8	18.43	6.75	49.5	53.68	18.71

Notations as in Table I; standard deviations of the means of pooled age domains included for comparison. Inhomogeneous precision levels of deconvolved σ errors reflect inhomogeneous dependences of the residuals

cluster averages, by programing the residuals by iteratively modifying the standard deviations of each age cluster. The optimization was directed towards minimization of the integral of the residuals while keeping their absolute value inside an envelope of $5e^{-4}$ probability units. The final integral of the residuals obtained was $4.73 \cdot 10^{-2}$, with a sum of squared residuals of $1.15 \cdot 10^{-3}$.

The refinement summarized in Table II allows the separation of the age clusters at a 95% confidence level using pooled age domains, while the deconvolved distribution functions resolve the same cluster separations at 1σ level.

The separated age clusters are consistent with inherited ages reflecting a regional metamorphic event rather poorly constrained around the Neoproterozoic-Cambrian boundary (528 ± 17.86 Ma), overprinted by pervasive Ordovician

contact metamorphism (462 ± 4.54 Ma). The corresponding main age cluster is consistent within error or slightly postdates the magmatic age (472.7 ± 7.3 Ma) of the adjacent Albești Metagranite [27]. Ages ranging from Silurian to Early Devonian, grouped in two maxima, indicate Early Paleozoic recrystallization episodes. The position of the older of the two maxima relative to the probability distribution function (Fig. 9, 10) and the good separation from the following maximum is also consistent with a duration of the thermal overprint of about 30 ± 7 Ma postdating the granite intrusion. The second maximum of this pair is located closer to the younger, well-defined and chemically homogeneous cluster at 371 Ma, which defines the early Variscan age of the pervasive medium- to high-pressure overprint responsible for the garnet-phengite-kyanite assemblage. This event is constrained to Late Devonian (371 ± 7.14 Ma). The minor age cluster located at 332 ± 7.14 Ma cluster is indicative of retrogression during late Variscan shallower-level stacking of partly exhumed units.

IV. Conclusions

The approach defined by [10] in chemical microprobe dating of monazite geochronology can be widely applied irrespective of context. However, the enhancements illustrated in this contribution seem essential to the authors, especially regarding error propagation tracking, consistently-scaled probability graphs, substantiated selection of coherent populations from random spot data, the assessment of supportive chemical data, and an effective procedure for deconvolution of complex spectra. The high spatial resolution of microprobe analyses and their in situ character offer, besides tracking precise location of the individual spots and a higher probability to get unmixed analyses, possibilities to relate age values to textural contexts and internal zonality of the grains. However, the connection between the textural setting or chemical zonality and age data is not always apparent, being circumstantial to identification of reaction textures and inclusion relationships.

Therefore, a thorough chemical characterization of the analyzed spot population is an independent criterion not only for distinction of coherent domains which can be related to time intervals, but also for the assessment of the variations inside each of these domains. The relationship between chemical features and age data represents in many instances a sensible insight in the petrogenetical evolution of minerals and rocks in time.

A practical way to relate chemical features with age data is plotting together ages, gradients inside a population, and chemical indices of the spot data, allowing continuous visual inspection of the data and enabling suitable data selection and grouping. Deconvolution of complex age spectra into geologically relevant components can be achieved with acceptable accuracy using combined chemical and statistical criteria, assisted by accurate graphical representations of the probability function.

Acknowledgements

Hans-Joachim Massonne is gratefully acknowledged for extensively granting access to the analytical facilities at the Institute of Mineralogy and Crystal Chemistry of the University in Stuttgart. Thomas Theye patiently assisted the authors in harnessing the microprobe, provided analytical help and seminal discussions not only during an Alexander von Humboldt institutional partnership, but also along the years preceding and following it.

References

[1] D. Rhede, I. Wendt, and H.-J. Förster, “A three-dimensional method for calculating independent chemical U/Pb- and Th/Pb-ages of accessory minerals”, *Chem. Geol.*, vol. 130, nr. 3-4, pp. 247-253, 1996.

[2] K. Suzuki, “CHIME dating and age mapping of monazite in granulites and paragneisses from the Hwacheon area, Korea: implications for correlations with Chinese cratons” , *Geosci. J.*, vol. 13, nr. 3, pp. 275-292, 2009

[3] R. R. Parrish, “U–Pb dating of monazite and its application to geological problems”, *Canad.. J. Earth Sci.*, vol. 27, nr. 11, pp. 1431-1450, 1990.

[4] N. C. Scherrer, M. Engi, E. Gnos, V. Jakob, and A. Liecht, “Monazite analysis: from sample preparation to microprobe age dating and REE quantification”, *Schweizer. Mineral. Petrogr. Mitt.*, vol. 80, pp. 93-105, 2000.

[5] J. M. Pyle, F.S. Spear, D. A. Wark, C. G. Daniel, and L. C. Storm, “Contributions to precision and accuracy of chemical ages of monazite”, *Amer. Mineral.*, vol. 90, pp. 547– 577, 2005.

[6] M. J. Jercinovic and M. L. Williams, “Analytical perils (and progress) in electron microprobe trace element analysis applied to geochronology: background acquisition interferences, and beam irradiation effects”, *Amer. Mineral.*, vol. 90, pp. 526-546, 2005.

[7] M. L. Williams, M. J. Jercinovic, D. E. Harlov, B. Budzyń, and C. J. Hetherington, “Resetting monazite ages during fluid-related alteration”, *Chem. Geol.*, vol. 283, nr. 3-4, pp. 218-225, 2011.

[8] A. M. Seydoux-Guillaume, R. Wirth, A. Deutsch, U. Schaerer, “Microstructure of 24-1928 Ma concordant monazites; implications for geochronology and nuclear waste deposits”, *Geochim. Cosmochim. Acta*, vol. 68, nr. 11, pp. 2517-2527, 2004.

[9] M. L. Williams, M. J. Jercinovic, P. Goncalves, and K. H. Mahan, “Format and philosophy for collecting, compiling, and reporting microprobe monazite ages”, *Chem. Geol*., vol. 225, nr. 1-2, pp. 1-15, 2006.

[10] J.-M. Montel, S. Foret, M. Veschambre, C. Nicollet and A. Provost, “Electron microprobe dating of monazite”, *Chem. Geol.*, vol. 131, nr. 1-4, pp. 37-53, 1996.

[11] K. Suzuki and M. Adachi, “Precambrian provenance and Silurian metamorphism of the Tsubonosawa paragneiss in the South Kitakami Terrane, Northeast Japan, revealed by the chemical Th-U-total Pb isochron ages of monazite, zircon and xenotime”, *Geochemical J.*, v. 25, pp. 357-376, 1991.

[12] A. Cocherie and F. Albarède, “An improved U-Th-Pb age calculation for electron microprobe dating of monazite”, *Geochim. Cosmochim. Acta*, vol. 65, nr. 24, pp. 4509-4522, 2001.

[13] A. Cocherie, E. Be Mezeme, O. Legendre, C. M. Fanning, M. Faure and P. Rossi, “Electron-microprobe dating as a tool for determining the closure of Th-U-Pb systems in migmatitic monazites”, *Amer. Mineral.*, vol. 90, nr. 4, pp. 607– 618, 2005.

[14] H. D. Gibson, S. D. Carr, M. A. Hamilton and R. L. Brown “Correlating Yttrium zones and age domains in monazite with metamorphic reactions involving major pelitic phases: an integration of IDTIMS and SHRIMP geochronology with Y-Th-U X-ray mapping” *Chem. Geol*., vol. 211, nr. 3-4, pp. 237-260, 2004.

[15] P. S. Dahl, M. A. Hamilton, M. J. Jercinovic, M. P. Terry, M. L. Williams and R. Frei, “Comparative isotopic and chemical geochronometry of monazite, with implications for U-Th-Pb dating by electron microprobe: An example from metamorphic rocks of the eastern

Wyoming Craton (U.S.A.)", *Amer. Mineral.*, vol. 90, nr. 4, pp. 619–638, 2005

[16] G. Săbău, "Chemical U-Th-Pb geochronology: a precise explicit approximation of the age equation and associated errors", *Geochronometria*, vol. 39, nr. 3, pp. 167-179, 2012.

[17] B. A. Wing, J. M. Ferry and T. M. Harrison, "Prograde destruction and formation of monazite and allanite during contact and regional metamorphism of pelites: petrology and geochronology", *Contrib. Mineral. Petrol.*, vol. 145, nr. 2, pp. 228-250, 2003.

[18] M. J . Kohn, M. S. Wieland, C. D. Parkinson and B. N. Upreti, "Five generations of monazite in Langtang gneisses: implications for chronology of the Himalayan metamorphic core", *J. metamorphic Geol*, vol. 23, nr. 5, pp. 399-466, 2003.

[19] J. Majka, Y. Be'eri-Shlevin, D. G. Gee , A. Ladenberger , S. Claesson, P. Konečný and I. Klonowska, "Multiple monazite growth in the Åreskutan migmatite: evidence for a polymetamorphic Late Ordovician to Late Silurian evolution in the Seve Nappe Complex of west–central Jämtland, Sweden", *J. Geosci*., nr. 57. vol. 1., pp. 3-23, 2012 .

[20] B. Rasmussen and J. R. Muhling, "Reactions destroying detrital monazite in greenschist-facies sandstones from the Witwatersrand basin, South Africa" *Chem. Geol.*, vol. 264, nr. 1-4, pp. 311-327, 2009.

[21] W. F. McDonough and S.-s. Sun, "The composition of the Earth", *Chem. Geol.*, vol. 120, nr. 3-4, pp. 223-253, 1995.

[22] T. Iizuka, M. T. McCulloch, T. Komiya, T. Shibuya, K. Ohta, H. Ozawa, E. Sugimura and K. D. Collerson, "Monazite geochronology and geochemistry of meta-sediments in the Narryer Gneiss Complex, Western Australia: constraints on the tectonothermal history and provenance", *Contrib. Mineral. Petrol.*, vol. 160, nr. 6, pp. 803-823, 2010.

[23] P. Goncalves, C. Nicollet and J.-M. Montel, "Petrology and in situ U–Th–Pb Monazite geochronology of ultrahigh-temperature metamorphism from the Andriamena Mafic Unit, north–central Madagascar. Significance of a petrographical P–T path in a polymetamorphic context", *Journ. of Petrology*, vol. 45, nr. 10, pp. 1923-1957, 2004.

[24] I. Braun, J.-M. Montel and C. Nicollet, "Electron microprobe dating of monazites from high-grade gneisses and pegmatites of the Kerala Khondalite Belt, southern India", *Chem. Geol.*, vol. 146, nr. 1-2, pp. 65-85, 1998.

[25] Ludwig K. R., "Isoplot 3.75 - A geochronological toolkit for Microsoft Excel", Berkeley Geochron. Center Special Publ. No. 5, rev. January 30, 75 pp., 2012

[26] E. Negulescu, *The significance of minerals and mineral assemblages in determining the metamorphic history of the crystalline basement of the Leaota Massif , "Semnificația mineralelor și a asociațiilor minerale în determinarea istoriei metamorfice a cristalinului Masivului Leaota"*, Iași: Tehnopress, 2013.

[27] I. Balintoni, C. Balica, M. N. Ducea, F. Chen, H. P. Hann and V. Șabliovschi, "Late Cambrian–Early Ordovician Gondwanan terranes in the Romanian Carpathians: A zircon U–Pb provenance study", *Gondwana Res*. vol. 16, nr. 1, pp. 119-133, 2009

Gavril Săbău (AM'12–M'13) was born in Lupeni, Hunedoara County, Romania, on July 20, 1956. He graduated in 1981 as engineer in geology and geophysics from the Faculty of Geology and Geography of the University in Bucharest, Section of Geological and Geophysical Engineering and obtained a *summa cum laude* PhD degree in 1999 at the University in Bucharest. His main field of study is mineralogy, petrology, geochemistry and geochronology of metamorphic rocks.

He performed state-mandated military service (1974-1975, 1981), rank at discharge second lieutenant, and has been employed with a state-owned prospecting company (1981-1983) as interim engineer in geology. Since 1983 he has been working with the Geological Institute of Romania as research geologist, head of department and deputy (scientific) director. Fellow of the Alexander von Humboldt Foundation (1992-1994). His present employment is senior researcher I and project manager with the Geological Institute of Romania in Bucharest.

Dr. Săbău is member of the Romanian Geological and Mineralogical Societies, Humboldt Club Romania, American Association for the Advancement of Science (AAAS), American Geophysical Union (AGU), and Geochemical Society. He was awarded the Ludovic Mrazec prize of the Romanian Academy (2002 – main author) and the prize of the Romanian Council for Research and Higher Education (2009 – coauthor).

Elena Negulescu (M'13) was born in Roșiori, Teleorman County, Romania, on May 4, 1968. She graduated in 1991 as engineer in geology from the Faculty of Geology of the University in Bucharest, Section of Geology and completed a PhD degree in 2007 at the University in Bucharest. Her main field of study is metamorphic petrology.

She was employed as a clerk until joining the Geological Institute of Romania in 1995as a research geologist. Her present employment is senior researcher with the Geological Institute of Romania in Bucharest.

Dr. Negulescu is member of the Romanian Geological and Mineralogical Societies, American Geophysical Union (AGU), and Geochemical Society. She was awarded the Ludovic Mrazec prize of the Romanian Academy (2002) and the prize of the Romanian Council for Research and Higher Education (2009) as a first author.